

EFFECT OF COMBINING PRECOMPRESSION GROOVES, PCFV AND DCFV ON PUMP NOISE GENERATION

Ganesh Kumar Seeniraj, Minming Zhao and Monika Ivantysynova

Purdue University, Department of Agricultural and Biological Engineering
 Maha Fluid Power Research Center, 1500 Kepner Drive, Lafayette, IN 47905, USA
 gseenira@purdue.edu, zhao90@purdue.edu, mivantys@purdue.edu

Abstract

Noise emission from axial piston machines has been studied for several decades by many researchers and pump manufacturers. As a result, different design methods for reducing the sources of pump noise have been proposed and are in use. The authors have studied and compared the effectiveness of several passive design methods. One of the outcomes of the study is the finding that among the passive design methods, precompression grooves and precompression filter volume (PCFV) are most effective in reducing the noise sources in the axial piston machines in a wide range of operating conditions. The limitations of precompression grooves and PCFV are explained and a new design method which combines the precompression grooves, PCFV and decompression filter volume (DCFV) has been proposed. The proposed combination of design methods is parameterized and uses a multi-objective optimization procedure. The effectiveness of the proposed optimization procedure (a combination of precompression grooves, PCFV and DCFV) is demonstrated using simulation results in comparison to precompression grooves and PCFV. The results show that a combination of precompression grooves, PCFV with groove and DCFV with groove, is effective in reducing both the fluid borne noise source (FBNS) and the structure borne noise source (SBNS) simultaneously in an axial piston machine at a wide range of operating conditions. It has also been shown that the proposed method allows noise source reduction without affecting volumetric efficiency.

Keywords: noise reduction, axial piston pump, combination, precompression grooves, precompression filter volume

1 Introduction

To achieve a quieter operation of any axial piston machine (Fig. 1) over the entire operating range, both the fluid borne noise source (FBNS) and the structure borne noise source (SBNS) need to be minimized simultaneously over the operating range instead of at one operating condition. FBNS is generally attributed to the flow pulsation in the discharge and suction ports of the pump. SBNS is attributed to the oscillating moments imparted on the swash plate about the three coordinate axes due to fluctuating pressure in the displacement chamber.

A multi-objective multi-parameter optimization procedure to simultaneously reduce FBNS and SBNS over the entire operating range of an axial piston machine has been proposed and validated using sound pressure level measurements (Seeniraj, 2009; Seeniraj and Ivantysynova, 2011).

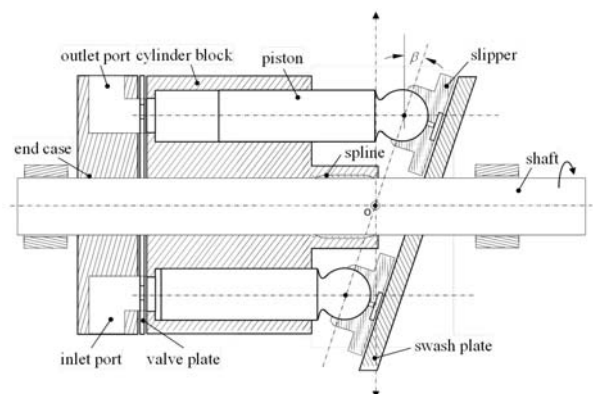


Fig. 1: Schematic of an axial piston swash plate pump

This manuscript was received on 01 October 2010 and was accepted after revision for publication on 28 September 2011

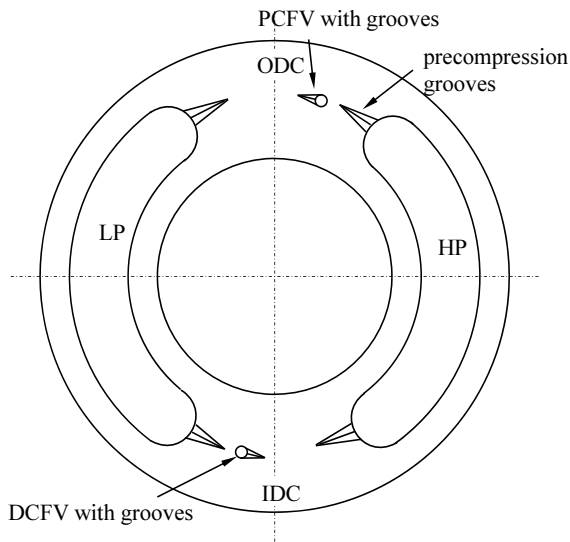


Fig. 2: Schematic of a valve plate with precompression grooves, PCFV with groove and DCFV with groove

In this work, the multi-objective optimization procedure has been extended to optimize the parameters of a valve plate with a combination of precompression grooves, precompression filter volume (PCFV) with grooves attached and decompression filter volume (DCFV) with grooves attached as shown in Fig. 2.

2 Precompression grooves, PCFV and DCFV

Reducing noise sources (FBNS and SBNS) in axial piston pump/motor mainly involves satisfying two conditions - (i) Facilitating a gradual transition of displacement chamber pressure from low to high pressure (compression) and vice versa (expansion) to increase the duration of the transition (Fig. 3); (ii) Keeping the reverse flow and the amplitude of the compressibility ripple (Fig. 4) to a minimum by compressing and expanding the fluid to the required high and low pressures respectively before the displacement chamber opens to the respective ports (Seeniraj, 2009).

Both of the mentioned tasks are typically achieved through valve plate modifications. Most of the passive design methods involving valve plate modification are sensitive to operating conditions and are effective only at a narrow operating range for which the valve plate is optimized. Among the passive methods, precompression grooves (Fig. 5) and precompression filter volume - PCFV (Fig. 6) have been proven to be less sensitive to operating conditions (Johansson, 2005; Seeniraj, 2009). Precompression grooves and PCFV have their advantages and limitations. All the earlier works in noise reduction in axial piston pumps have handled the compression and expansion inside the displacement chamber as separate processes. In general, works which focus on the slope of pressure rise in the displacement chamber, during transition from suction to discharge stroke, detail the factors that affect the slope of pressure and the reduction of flow pulsation in the discharge port (ΔQ_{HP}) and the amplitude of oscillating moment on

the swash plate (ΔM_X). Similarly, works which focus on the rate of expansion (transition from discharge to suction stroke), detail the factors which affect the expansion and the reduction of flow pulsation in the suction port (ΔQ_{LP}) and avoiding cavitation at the beginning of the suction stroke. This has been the state of the art even with the latest works including Johansson (2005) and Ericson (2008). But for the first time, in this work, the processes of precompression and expansion have been studied simultaneously and their effect on flow pulsations (ΔQ_{HP} & ΔQ_{LP}) and oscillating swash plate moments about all the three axes ($\Delta M_{X,Y,Z}$) are investigated.

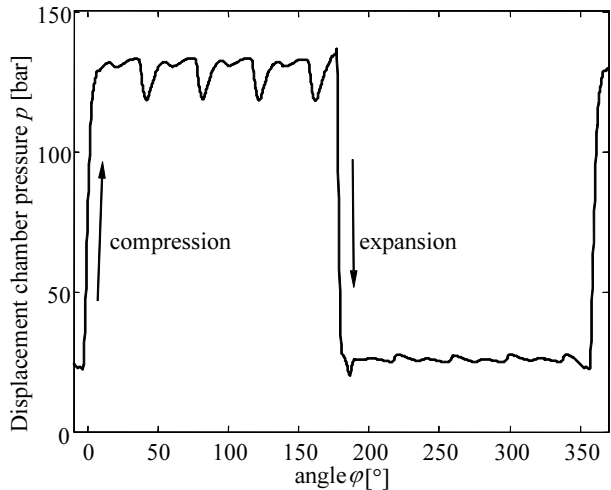


Fig. 3: Plot of simulated displacement chamber pressure over one shaft revolution

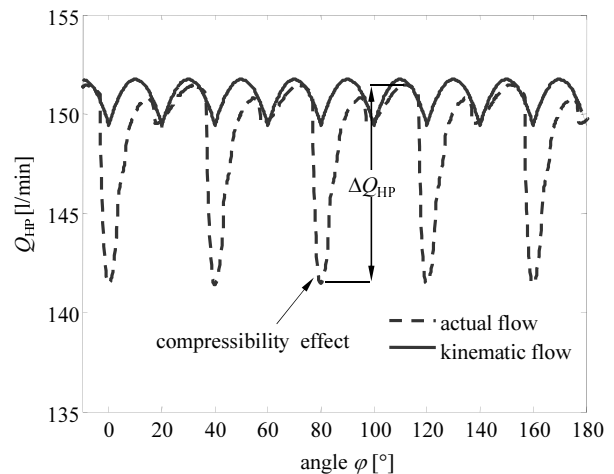


Fig. 4: Plot of simulated pump discharge flow showing the compressibility effect and amplitude of the ripple (ΔQ_{HP})

Precompression grooves can be optimized to make the pressure transition gradual. The longer and more controlled the opening of the groove, the slower is the transition. But longer grooves increase the cross port leakage in cases where cross porting is allowed (Seeniraj 2009). Also, the amplitude of the flow pulsation is tightly linked to the compression of the fluid while using precompression grooves (Johansson, 2005). Conse-

quently, precompression grooves make flow ripples highly sensitive to operating condition.

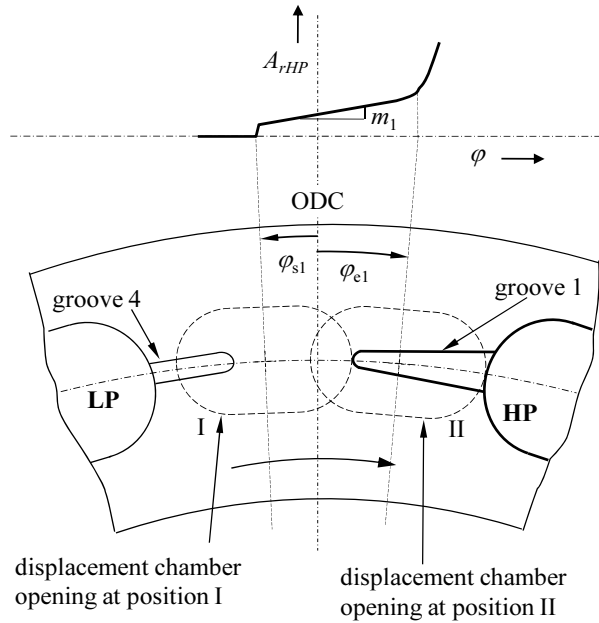


Fig. 5: An exemplified section of valve plate having grooves near outer dead center. The parameters of groove 1 (ϕ_{s1} , ϕ_{e1} and m_1) are shown along with the area it represents (A_{rHP}) (Seeniraj, 2009)

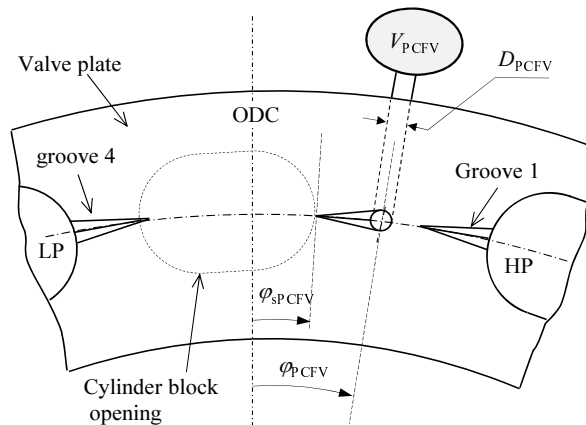


Fig. 6: A exemplified section of valve plate with a PCFV attached near the outer dead center. The parameters of PCFV (ϕ_{sPCFV} , ϕ_{PCFV} and V_{PCFV}) are also shown

On the other hand, PCFV decouples the compression and amplitude of the flow pulsation (Johansson, 2005) and hence PCFV is effective in reducing flow pulsations over a wide range of operating conditions. But PCFV increases the rate of compression and consequently SBNS (Ivantysynova et al., 2005; Seeniraj, 2009). The idea of combining the two methods was arrived from the results of an investigation where the PCFV was attached to a valve plate which already had grooves as presented in Ivantysynova et al. (2005). Interestingly the same idea of combining the relief grooves with PCFV is presented in Johansson and Palmberg (2005). PCFV affects the rate of pressure rise in the displacement chamber during transition from suction to discharge stroke near the outer dead centers (ODC) of the pistons. A similar volume, named de-

compression filter volume (DCFV), affecting the rate of expansion, can be provided at the inner dead center (IDC) of piston during the transition from discharge to suction stroke.

Unlike the previous works, in this research, both compression and expansion were optimized simultaneously. Details on the need to optimize compression and expansion simultaneously can be found in Seeniraj (2009). Most of the applications that employ axial piston units (pumps/motors) require the units to operate in a wide range of operating conditions as well as in both pumping and motoring mode. This requirement necessitates the valve plate be symmetric with respect to outer and inner dead centers (ODC and IDC) allowing the unit to work in pumping as well as in motoring mode. This requirement was kept in mind while studying the effectiveness of a combination of precompression grooves, precompression filter volume (PCFV) and DCFV. A symmetric valve plate with four precompression grooves, PCFV with groove and DCFV with groove) is shown in Fig. 2.

3 Computer Aided Multi-objective Optimization

A multi-parameter multi-objective optimization procedure originally proposed and tested to optimize the precompression groove parameters (Seeniraj, 2009; Seeniraj and Ivantysynova, 2011) has been extended in this research work to study the effectiveness of the combined design method which involves the precompression groove, the PCFV with grooves and the DCFV with grooves. The multi-objective optimization of 6 objectives (representing FBNS and SBNS) and n parameters can be formulated as follows:

Minimize $(\Delta Q_{HP}, \Delta Q_{LP}, \Delta M_X, \Delta M_Y, \Delta M_Z, Q_{LK}) = \mathbf{x}$
where $\mathbf{x} = [x_1 \dots x_n]^T$

$$\text{s.t. } x_i^l \leq x_i \leq x_i^h \quad i = 1 \dots n \quad (1)$$

with no cavitation and no over-pressurization where \mathbf{x} is a vector of valve plate parameters (detailed in the next section) with each parameter having a range of values from x_i^l to x_i^h .

The mathematical model of the axial piston pump used in the heart of the optimization procedure is detailed here. The pump has z displacement chambers. Each displacement chamber is simulated and their effects summed up to simulate the entire pump. The rate of change in pressure inside each displacement chamber (dp/dt) can be calculated using a control volume approach (Fig. 7).

$$\frac{dp}{dt} = -K \frac{vA - Q_i - Q_s}{V_0 - sA} \quad (2)$$

where K is the fluid bulk modulus, v piston velocity, A piston cross sectional area, s piston displacement, V_0 piston volume at ODC, Q_i the sum of the flow rates between of the i^{th} displacement chamber and the pump ports and Q_s the sum of leakage through three different lubricating gaps between piston-cylinder (Q_{SK}), cylinder block-valve plate (Q_{SB}) and slipper-swash plate

(Q_{SG}) (Ivantysyn and Ivantysynova, 2001). The effect of change in relief groove geometry on the leakages through the lubricating gaps is negligible. As the optimization only changes the relief groove, the leakage in the lubricating gaps is assumed to remain the same for all the designs compared in the optimization and hence Q_S is eliminated from Eq. 2. Q_{ri} can be expressed as,

$$Q_{ri} = Q_{rHPi} + Q_{rLPi} \quad (3)$$

where Q_{rHPi} is the flow rate between the i^{th} displacement chamber and the discharge port and Q_{rLPi} the suction port and can be expressed using the orifice flow relationship.

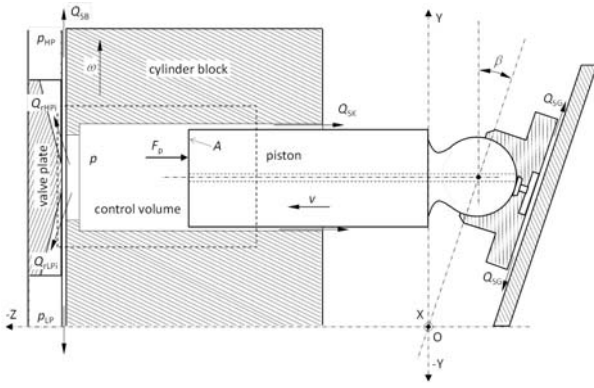


Fig. 7: Control volume for evaluating the pressure inside the displacement chamber

$$Q_{rHPi} = \alpha_D A_{rHP} \sqrt{\frac{2}{\rho} |p_{HP} - p_i| \text{sgn}(p_{HP} - p_i)} \quad (4)$$

$$Q_{rLPi} = \alpha_D A_{rLP} \sqrt{\frac{2}{\rho} |p_{LP} - p_i| \text{sgn}(p_{LP} - p_i)} \quad (5)$$

where α_D is the discharge coefficient, A_{rHP} and A_{rLP} is the valve plate opening areas available for flow transfer between the displacement chamber and the pump ports (Fig. 7), ρ fluid density, p_{HP} pressure at pump outlet and p_{LP} pressure at pump inlet.

V_0 in Eq. 2, the volume of the displacement chamber at the ODC when the piston is fully drawn out of the cylinder block, can be expressed as

$$V_0 = V_D + AR(\tan \beta_{max} + \tan \beta) \quad (6)$$

where V_D is the dead volume in the displacement chamber and β_{max} the maximum swash plate angle. The flow rate at the pump outlet (Q_{HP}) and inlet (Q_{LP}) are obtained by summing up the flow rate from the individual displacement chambers.

$$Q_{HP} = \sum_{i=1}^z Q_{rHPi} \quad (7)$$

$$Q_{LP} = \sum_{i=1}^z Q_{rLPi} \quad (8)$$

The pressure in the displacement chamber is further used to evaluate the forces exerted on the swash plate and the moments created due to the forces. According to Ivantysyn and Ivantysynova (2001), the total force on each piston can be expressed as,

$$F_{Ai} = F_p + F_f + F_a \quad (9)$$

where F_{Ai} is the sum of the pressure force (F_p), friction force between the piston and the cylinder block (F_f) and the force due to acceleration of the piston (F_a). The normal components of the force due to each piston on the swash plate F_{NSi} and F_{Nyi} are responsible for creating the moment about the X-axis (Fig. 8).

$$F_{NSi} = \frac{F_{Ai}}{\cos \beta} \quad (10)$$

$$F_{Syi} = -F_{NSi} \sin \beta = -F_{Ai} \tan \beta \quad (11)$$

$$M_x = \frac{R}{\cos^2 \beta} \sum_{i=1}^z F_{Ai} \cos \phi_i \quad (12)$$

$$M_y = R \sum_{i=1}^z F_{Ai} \sin \phi_i \quad (13)$$

$$M_z = -R \tan \beta \sum_{i=1}^z F_{Ai} \sin \phi_i \quad (14)$$

The individual forces due to each piston can be summed up and the moment created due to these the forces about the coordinate axis can be evaluated as described below. The relations, in Eq. 12 to 14, determine the moments about the three coordinate axes and depend upon the pressure inside the displacement chamber (p), the angular position of each piston (ϕ_i) and the swash plate angle (β).

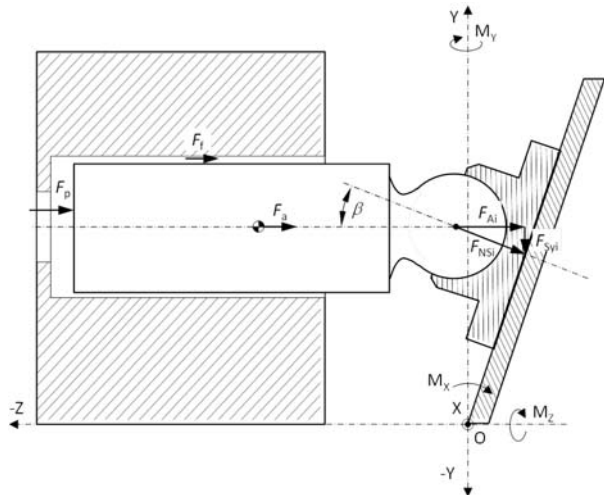


Fig. 8: Moments on the swash plate

The fluid density and bulk modulus used in this simulation are temperature and pressure dependent as expressed through the following relationships where bulk modulus K is defined as the reciprocal of the isothermal coefficient of compressibility (β_p).

$$\rho(T) = r_s (1 - a_{1s} T) \quad (15)$$

$$\rho(p, T) = \frac{\rho(T)}{1 - a_1 \ln \left(\frac{a_2 - a_2 T + p}{a_2 + a_{2T}} \right)} \quad (16)$$

$$K = \frac{1}{\beta_p(p, T)} = \frac{\rho(T)(a_2 + a_3 T + p)}{a_3 \rho(p, T)} \quad (17)$$

The values of the coefficients in Eq. 15 to 17 are listed here for oil type HLP32.

$$\begin{aligned}
 a_1 &= 0.07329654 \\
 a_2 &= 1965.018 \text{ bar} \\
 a_3 &= -2.968126 \text{ bar/K} \\
 r_s &= 1047.03 \text{ kg/m}^3 \\
 a_{1s} &= 0.0005761668 \text{ 1/K}
 \end{aligned}$$

As shown in Fig. 6, the PCFV has been modeled as a fluid volume attached to the valve plate (Ivantsynova et al., 2005). The pressure and flow rate in/out of the PCFV can be expressed as follows.

$$\frac{dp_{PCFV}}{dt} = -\frac{K}{V_{PCFV}} [Q_{rPCFV}] \quad (18)$$

$$Q_{rPCFV} = -\alpha_D A_{PCFV} \sqrt{\frac{2}{\rho}} \sqrt{p - p_{PCFV} \operatorname{sgn}(p - p_{PCFV})} \quad (19)$$

A_{PCFV} is the area available for flow exchange between the PCFV and the displacement chamber and this area is defined by the parameters 13 to 17 listed in Table 1. The mathematical model is implemented using C++ programming language and differential equations are numerically solved using explicit Runge-Kutta method of order 5 due to Dormand & Prince with step size control. The C++ class for the implementation of Runge-Kutta method used in this work is taken from Ashby (2002).

All the parameters for the proposed new valve plate (Fig. 2 and 6) with precompression grooves, PCFV with grooves and DCFV with grooves are listed in Table 1 with proposed initial ranges. The angular locations associated with the PCFV and the DCFV are 180 degrees apart keeping them symmetric with respect to corresponding dead centers. Keeping the symmetry significantly reduces the number of designs in the initial solution space. In particular cases, where the axial piston unit operates only as a pump or a motor, the symmetry constraint can be removed to include unsymmetrical designs in the search for the optimal design. Though the proposed multi-objective optimization procedure is fully capable of optimizing an unsymmetrical case, it has not been presented in this paper. During the optimization, designs were selected based on Pareto optimality of three objectives ΔQ_{HP} , ΔQ_{LP} and ΔM_X . Q_{LK} was involved as a trade-off objective in the higher-level decision making during the final stages of selecting the optimal design. During the course of this research, it was observed that the profiles of M_Y and M_Z are strongly correlated to the profiles of flow ripples at high and low pressure ports. Consecutively, the trends of ΔM_Y and ΔM_Z are similar to ΔQ_{HP} and ΔQ_{LP} . It implies that designs with lower ΔQ_{HP} and ΔQ_{LP} would also have lower ΔM_Y and ΔM_Z . Hence ΔM_Y and ΔM_Z are not included explicitly in selecting the Pareto optimal designs. The steps involved in the multi-objective optimization procedure have been detailed in Seeniraj (2009) and an overview of the procedure is presented in Fig. 9.

Table 1: List of parameters for the valve plate shown in Fig. 2 and 6

| | Parameters | Symbol | Initial range | Unit |
|----|--------------------------------------|----------------|---------------|----------------------|
| 1 | Starting location of groove 1 | ϕ_{s1} | 4-7 | [°] |
| 2 | Starting location of groove 3 | ϕ_{s3} | 184-187 | [°] |
| 3 | Starting location of groove 2 | ϕ_{s2} | 174-177 | [°] |
| 4 | Starting location of groove 4 | ϕ_{s4} | 354-357 | [°] |
| 5 | Ending location of groove 1 | ϕ_{e1} | 11-14 | [°] |
| 6 | Ending location of groove 3 | ϕ_{e3} | 191-194 | [°] |
| 7 | Ending location of groove 2 | ϕ_{e2} | 175-178 | [°] |
| 8 | Ending location of groove 4 | ϕ_{e4} | 355-358 | [°] |
| 9 | Slope of groove 1 | m_1 | 0.3-0.6 | [mm ² /°] |
| 10 | Slope of groove 3 | m_3 | 0.3-0.6 | [mm ² /°] |
| 11 | Slope of groove 2 | m_2 | 0-0.06 | [mm ² /°] |
| 12 | Slope of groove 4 | m_4 | 0-0.06 | [mm ² /°] |
| 13 | Starting location of the PCFV groove | ϕ_{sPCFV} | 352-355 | [°] |
| 14 | Location of the PCFV port | ϕ_{PCFV} | 5-8 | [°] |
| 15 | Size of the PCFV | V_{PCFV} | 75 | [cc] |
| 16 | Slope of the PCFV groove | m_{PV} | 0.2-0.4 | [mm ² /°] |
| 17 | Diameter of the PCFV | D_{PCFV} | 1.6 | [mm] |
| 18 | Starting location of the DCFV groove | ϕ_{sDCFV} | 172-175 | [°] |
| 19 | Location of the DCFV port | ϕ_{DCFV} | 185-188 | [°] |
| 20 | Slope of the DCFV groove | m_{DV} | 0.2-0.4 | [mm ² /°] |
| 21 | Size of the DCFV | V_{DCFV} | 75 | [cc] |
| 22 | Diameter of the DCFV | D_{DCFV} | 1.6 | [mm] |

The initial range of parameters listed in Table 1 is where the optimization was started. The initial range of values for each parameter is based on a prior investigation where each parameter was studied in a wider range and the effect of each parameter value on all the objectives (Seeniraj, 2009). As the investigation matured, the range of values with in which the parameters are allowed to vary was finalized.

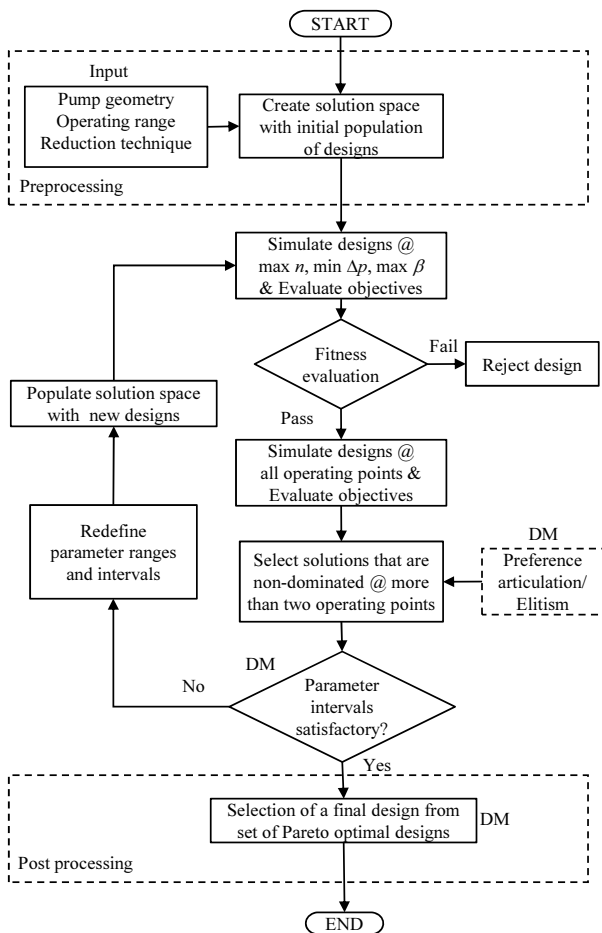


Fig. 9: Flow chart representation of the multi-objective optimization procedure

4 Effectiveness of Combining Pre-compression Grooves, PCFV and DCFV

The main goal of this paper is to explain and demonstrate the effectiveness of combining precompression grooves, PCFV with grooves and DCFV with grooves on pump noise generation over conventional designs. To do that, three valve plates (VP1, VP2 and VP3) have been compared in this section.

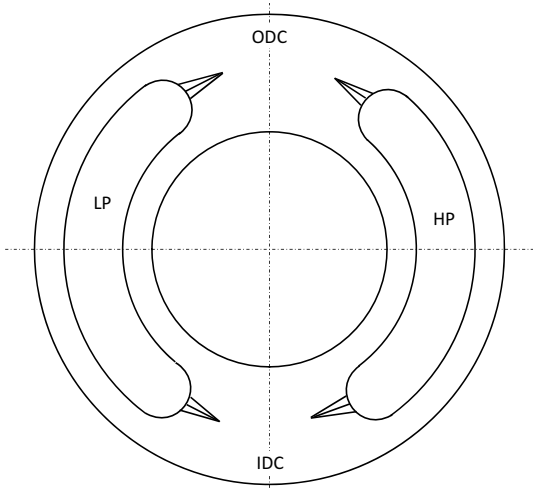


Fig. 10: Valve plate 1 (VP1) optimized for precompression grooves

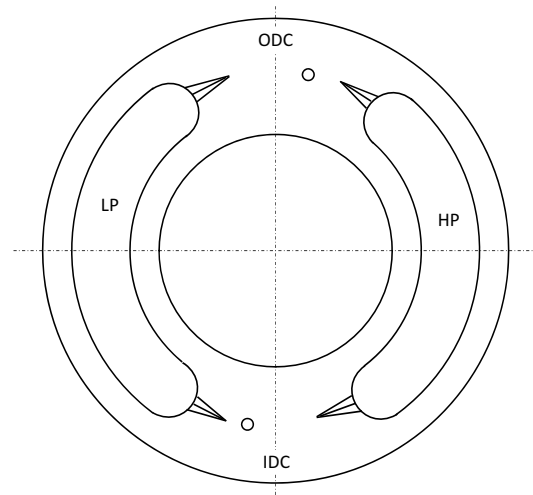


Fig. 11: Valve plate 2 (VP2) optimized for precompression grooves, PCFV and DCFV

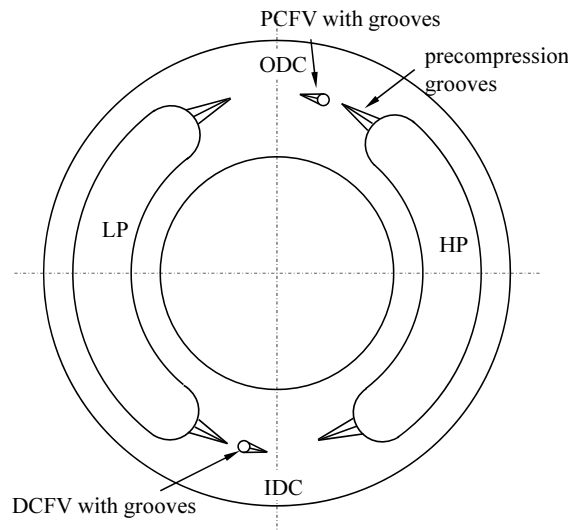


Fig. 12: Valve plate 3 (VP3) with precompression grooves, PCFV with groove and DCFV with groove

VP1 (shown in Fig. 10) is a valve plate with four precompression grooves. VP1 has been optimized in a previous study for noise using the multi-objective optimization procedure (Seeniraj and Ivantysynova, 2011).

VP2 (shown in Fig. 11) is a valve plate with four precompression grooves, a PCFV and a DCFV. VP2 does not have a leading groove attached to the PCFV and the DCFV.

VP3 (shown in Fig. 11) is a valve plate which has four precompression grooves, a PCFV with a leading groove and a DCFV with a leading groove.

The three valve plates (VP1, VP2 and VP3) have been separately optimized for an axial piston pump of size 75 cc having 9 pistons operating with pressure from 100 to 400 bar, rotational speed from 1000 to 3000 rpm and displacement from 20 % to 100 %. The optimization was achieved using the multi-objective optimization procedure represented in Fig. 9. For detailed explanation of the optimization procedure, refer Seeniraj and Ivantysynova (2011).

A comparison of the three valve plates in terms of the 6 objectives of the optimization at 12 operating conditions is presented in the following passages. The 6 objectives are the amplitude of flow pulsation in discharge and suction ports (ΔQ_{HP} , ΔQ_{LP}); the amplitude of oscillating swash plate moments about the three axes (ΔM_X , ΔM_Y , ΔM_Z) and the volumetric loss due to compression and cross flow leakage (Q_{LK}). The 12 operating conditions include 2 different operating pressures, 3 rotational speeds and 2 displacements.

In Fig. 13 to 17, the three valve plates are differentiated using different marker shapes. The marker colour indicates the operating condition shown on the colour bar. The colour bar text lists the operating conditions in an abbreviated form. For example, the legend ‘p100n1000’ is the abbreviation for ‘pressure (p) 100 bar and rotational speed (n) 1000 rpm. The plots presented in this section need to be viewed in colour for clarity.

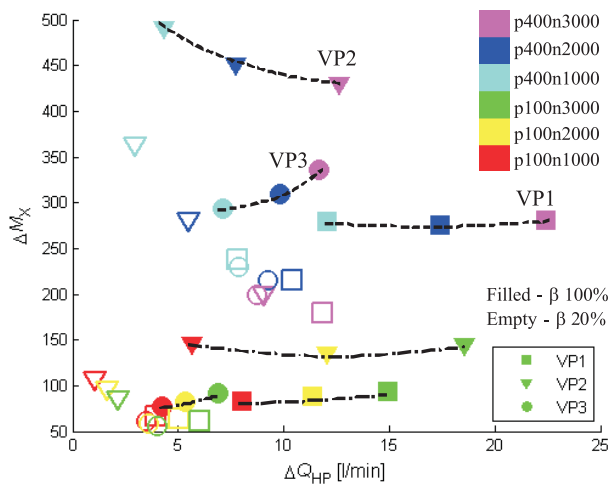


Fig. 13: Plot of simulated objectives ΔQ_{HP} versus ΔM_X for VP1, VP2 and VP3 at 12 operating conditions

Figure 13 shows the objective ΔQ_{HP} plotted against ΔM_X for the three valve plates at 12 different operating conditions. The dashed lines represent the trend of objectives at an operating pressure of 400 bar and displacement of 100 % over three different rotational speeds. Similarly, the dashed-dotted lines represent the trend at a pressure of 100 bar and displacement of 100% over three different rotational speeds.

From the results presented in Fig. 13 and 14, the following conclusions can be drawn regarding the fluid-borne noise source (flow pulsations ΔQ_{HP} and ΔQ_{LP}) and structure-borne noise source (oscillating moment ΔM_X).

VP1 represents a valve plate optimized using only pre-compression grooves. As explained in Section 2, pre-compression grooves are effective in reducing the rate of compression and expansion and hence VP1 has lower ΔM_X at all operating conditions (Fig. 13). But the reduction in ΔM_X comes at the cost of flow ripple. VP1 has the largest flow ripple (ΔQ_{HP} and ΔQ_{LP}) among the three compared valve plates at all operating conditions (Fig. 14).

VP2 optimized using PCFV and DCFV (without attached grooves) is effective in reducing the flow pulsations. VP2 has lower flow pulsations than VP1 at all operating points (Fig. 14). VP2 also has lower flow pulsations than VP3 at most but not all operating conditions.

As explained in Section 2, PCFV increases the rate of compression and hence increases the amplitude of the swash plate moments. Consequently, VP2 has the largest ΔM_X at all operating conditions.

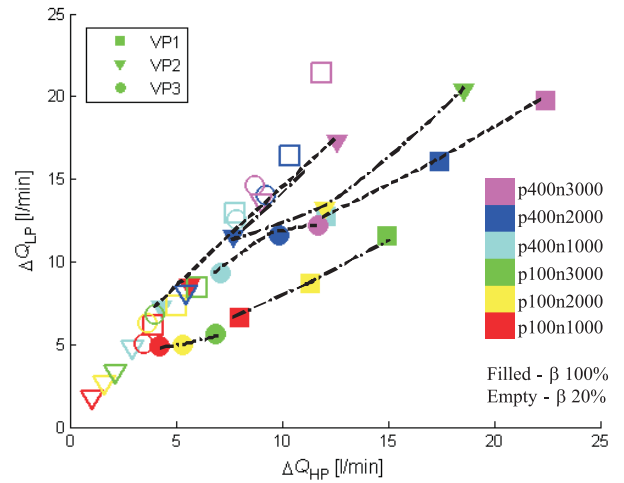


Fig. 14: Plot of simulated objectives ΔQ_{HP} versus ΔQ_{LP} for VP1, VP2 and VP3 at 12 operating conditions

VP3 takes advantage of the properties of pre-compression grooves, PCFV and DCFV in reducing both flow ripples and swash plate moments. VP3 matches the effectiveness of VP2 in reducing ΔQ_{HP} and ΔQ_{LP} and VP1 in reducing ΔM_X . It should be noted that at high power operating regions (high pressure, high speed, and full displacement) VP3 is better than VP1 and VP2 in all the three objectives (ΔQ_{HP} , ΔQ_{LP} and ΔM_X).

The trend of the other two objectives ΔM_Y and ΔM_Z can be observed in Fig. 15 and 16. The trends of ΔM_Y and ΔM_Z are conflicting with ΔM_X . VP1 which had the lowest ΔM_X has the highest ΔM_Y and ΔM_Z . The inverse applies for VP2. VP3 is in the middle with smaller ΔM_Y and ΔM_Z than VP1 and smaller ΔM_X than VP2.

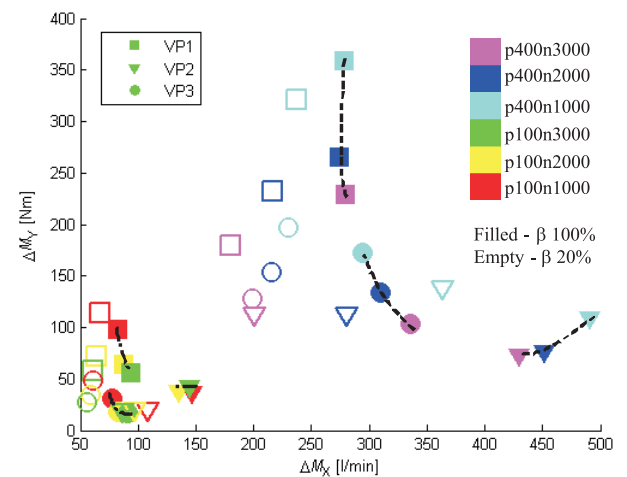


Fig. 15: Plot of simulated objectives ΔM_X versus ΔM_Y for VP1, VP2 and VP3 at 12 operating conditions

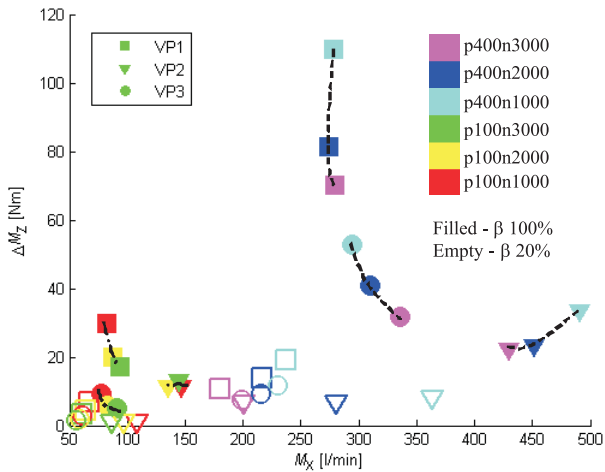


Fig. 16: Plot of simulated objectives ΔM_X versus ΔM_Z for VP1, VP2 and VP3 at 12 operating conditions

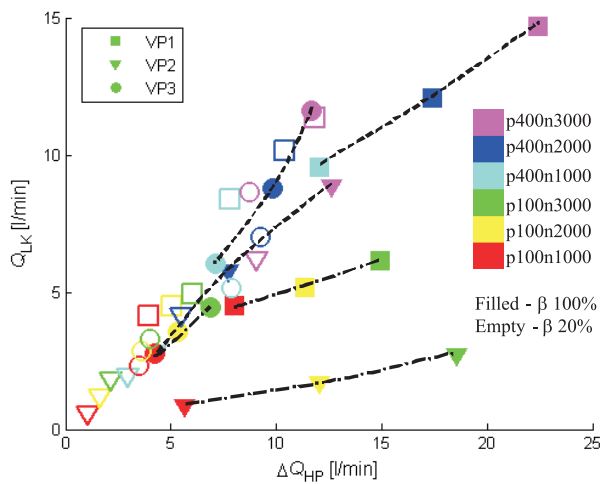


Fig. 17: Plot of simulated objectives ΔQ_{HP} versus ΔQ_{LK} for VP1, VP2 and VP3 at 12 operating conditions

For VP3, the quantitative reduction in ΔM_X is much higher than the increase in ΔM_Y and ΔM_Z when compared to VP2. As explained in the end of Section 3, the trends objectives ΔM_Y and ΔM_Z follow the trends of ΔQ_{HP} and ΔQ_{LP} . Hence, observing Fig. 13 to 16, it can be concluded that VP3 is better than VP1 and VP2 when comparing all the five objectives ΔQ_{HP} , ΔQ_{LP} , ΔM_X , ΔM_Y and ΔM_Z in most operating conditions and especially in high power operating regions.

From Fig. 17, VP1 and VP3 have higher volumetric loss than VP2 at all operating conditions. This is because VP1 and VP3 have higher cross port angles and consequently higher cross port leakages than VP2. During this particular optimization cycle, the leakage objective Q_{LK} was always traded off over all other objectives. It should be noted that, VP3 with improvements in all the noise objectives, still has lower leakage than VP1.

As it was an initial attempt at optimizing a large number of parameters, the authors tolerated a loss in efficiency over reduction in both FBNS and SBNS. A further optimization study was taken up to investigate the possibilities of reducing the cross port leakage without having to sacrifice on noise objective. The results of the optimization study with reduction in noise as well as cross port leakage are presented in the section 5.

5 Reduction in Cross Port Leakage

A different industrial pump of size 46 cc with 9 pistons was chosen for the study to reduce the cross port leakage. The valve plate of the 46 cc pump is similar to the valve plate VP2 shown in Fig. 11 and this industrial valve plate will be referred to as Standard in this section. The pump was subject to the multi-objective optimization and an optimal valve plate (similar to VP3 in Fig. 12) with the combination of precompression grooves, PCFV with leading groove and DCFV with leading groove was selected at the end of the optimization procedure. During the whole process, the cross porting was kept less than 3 degrees unlike the previous study where the cross port was varied up to 15 degrees. The valve plate with combined design methods resulted from the optimization procedure will be referred to as the Optimal in this section. Figure 18 shows the valve plate opening areas for the Optimal design. Figure 19 shows a magnified plot of the valve plate opening areas of the Optimal design near the inner dead center where the displacement chamber transitions from discharge to suction stroke.

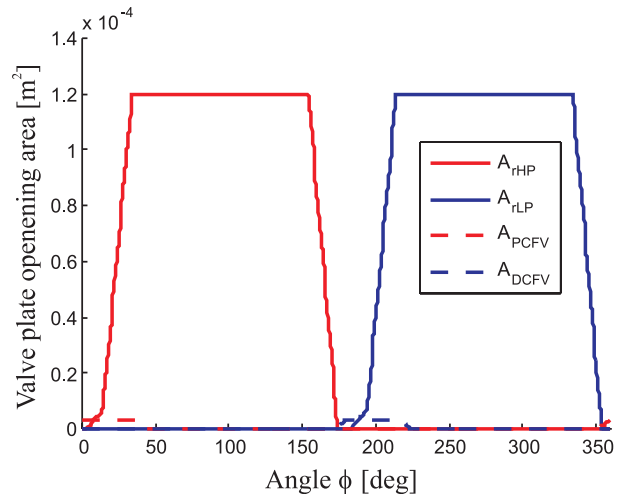


Fig. 18: Plot of valve plate opening areas for the 'Optimal' design

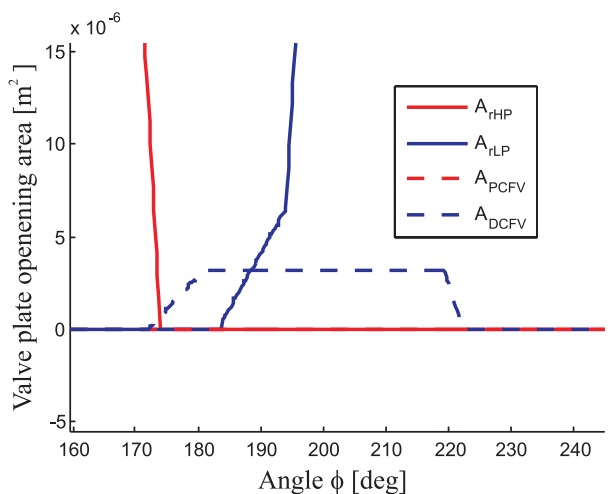


Fig. 19: Plot of valve plate opening areas for the 'Optimal' design near the IDC (transition from discharge to suction stroke)

Figures 20 to 22 show the plot of simulated flow pulsations and swash plate moments for the Standard and the Optimal designs at 350 bar, 100 % displacement and 3000 rpm for one complete shaft revolution.

Figures 23 to 27 show the comparison between valve plates Standard (similar to Fig. 11) and Optimal (similar to Fig. 12) for all the objectives (ΔQ_{HP} , ΔQ_{LP} , ΔQ_{LK} , ΔM_X , ΔM_Y and ΔM_Z) at eight different operating conditions. The marker and color schemes are similar to the previous section. The arrows in Fig. 23 to Fig. 27 accentuate the reduction in objective between the two designs. For example, in Fig. 23, at p400n3000 - β 100 %, the Optimal has the same ΔM_X but ΔQ_{HP} has been reduced more than 50 % of Standard. At the same operating condition, Optimal has also lower ΔQ_{LP} , ΔM_Y and ΔM_Z and a marginal increase in leakage (Fig. 24 to 27).

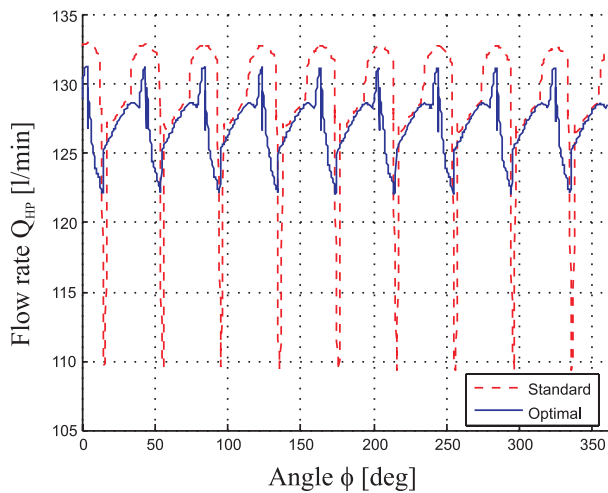


Fig. 20: Plot of simulated discharge flow for Standard and Optimal at Δp : 350 bar; n : 3000 rpm and β : 100 %

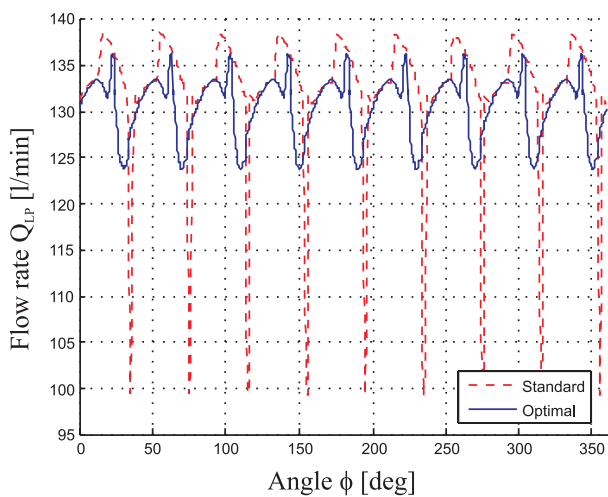


Fig. 21: Plot of simulated suction flow for Standard and Optimal at Δp : 350 bar; n : 3000 rpm and β : 100 %

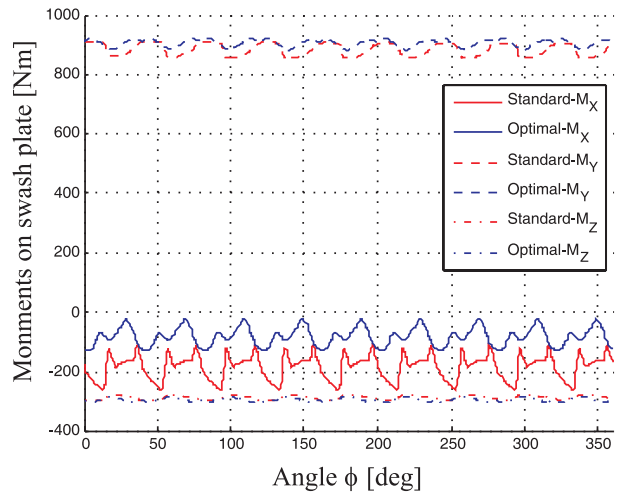


Fig. 22: Plot of simulated swash plate moments for Standard (solid) and Optimal (dashed) at Δp : 350 bar; n : 3000 rpm and β : 100 %

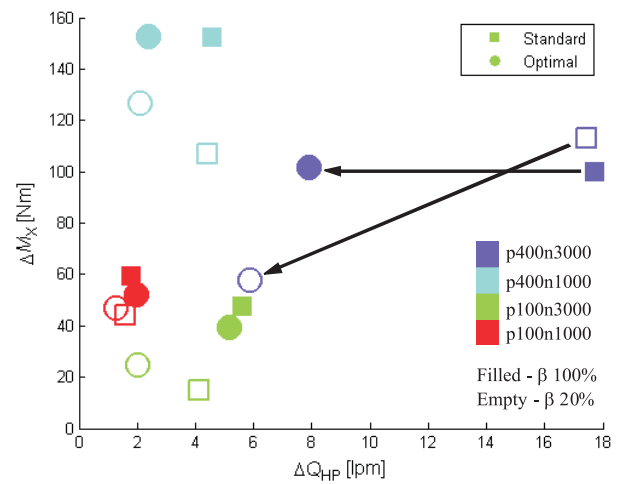


Fig. 23: Plot of simulated objectives ΔQ_{HP} versus ΔM_X for Standard and Optimal at 8 operating conditions

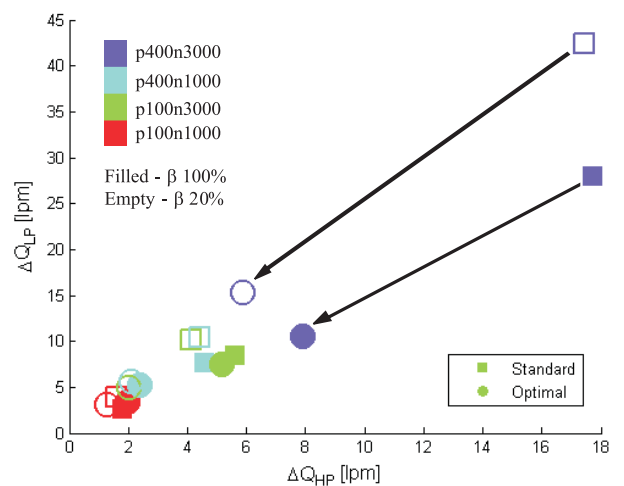


Fig. 24: Plot of simulated objectives ΔQ_{HP} versus ΔQ_{LP} for Standard and Optimal at 8 operating conditions

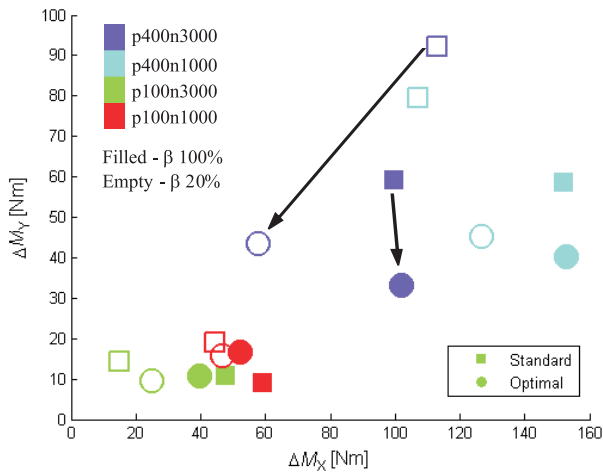


Fig. 25: Plot of simulated objectives ΔM_x versus ΔM_y for Standard and Optimal at 8 operating conditions

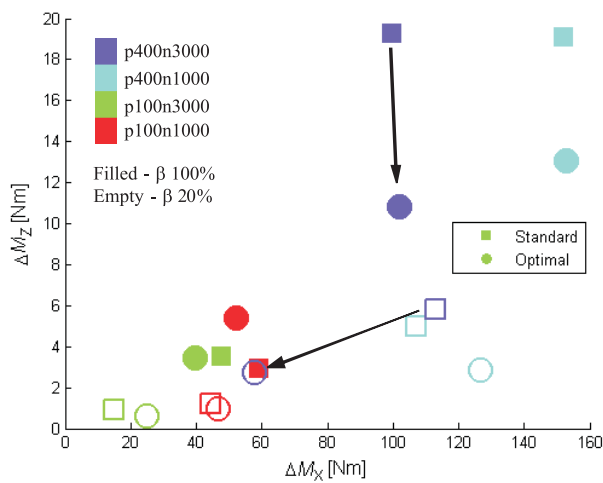


Fig. 26: Plot of simulated objectives ΔM_x versus ΔM_z for Standard and Optimal at 8 operating conditions

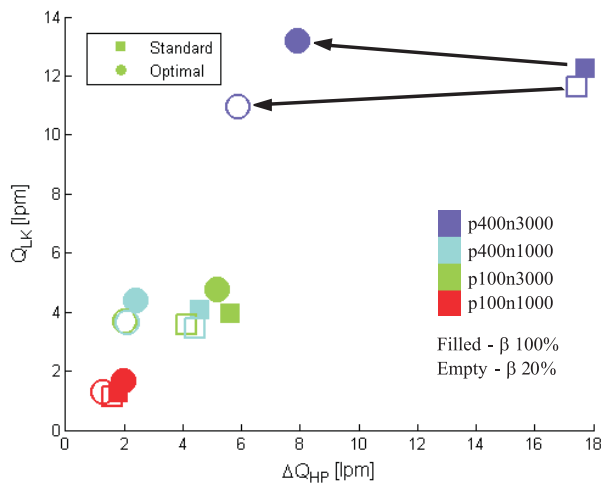


Fig. 27: Plot of simulated objectives ΔQ_{HP} versus ΔQ_{LK} for Standard and Optimal at 8 operating conditions

Optimal is better than Standard in all the noise objectives in most of the compared operating conditions. Optimal has marginally higher leakage than Standard in few operating conditions which is acceptable considering the reduction in noise objectives. Also, the acceptance or rejection of any design depends on the specific

system and on the trade-off preferred by the designer. The large reduction in all the noise objectives clearly shows the effectiveness of the Optimal over the Standard. It has been already proven by previous works that reducing both sources of noise brings down the overall airborne noise levels (Seeniraj, 2009 and Klop and Ivantysynova, 2010). The proposed optimal combination of grooves, PCFV and DCFV with its large reduction in noise objectives has a potential to be the quietest of among all the passive design methods.

6 Conclusions

In this paper, a previously developed multi-parameter multi-objective optimization scheme was extended to handle the combination of two different design approaches in a new simultaneous fashion. The algorithm/procedure was applied to optimize two existing standard industrial valve plates. The multi-objective optimization procedure applied in this work simultaneously optimizes the compression and expansion regions in the valve plate. Consequently both FBNS and SBNS are optimized simultaneously. It has also been shown that the volumetric efficiency of the pump is marginally affected while reducing the noise sources. The optimization procedure also allows for reduction in noise sources not just one operating condition rather the broad operating range of the axial piston unit. The optimization procedure detailed in this work has been developed into a software tool to assist designer to optimize pumps/motors with low noise sources. The optimization procedure has been already verified in a previous work. An experimental validation of the prototype of the proposed combination of design methods is planned in the near future.

Nomenclature

| Symbol | Description | Unit |
|-----------------|---|----------------------|
| α_D | Orifice discharge coefficient | - |
| β | Pump displacement | [%] |
| Δ | Peak-to-peak variation | - |
| φ | pump rotation angle | [°] |
| ρ | fluid density | [kg/m ³] |
| A | piston cross sectional area | [m ²] |
| A_{DCFV} | flow area available between displacement chamber and PCFV | [m ²] |
| A_{PCFV} | flow area available between displacement chamber and DCFV | [m ²] |
| A_{THP} | flow area available between displacement chamber and discharge port | [m ²] |
| A_{rLP} | flow area available between displacement chamber and suction port | [m ²] |
| F_{pi} | pressure force exerted by single piston on the swash plate | [N] |
| K | fluid bulk modulus | [Pa] |
| M_x, M_y, M_z | swash plate moment about the respective axes | [Nm] |
| p | displacement chamber pressure | [bar] |
| p_{HP} | discharge port pressure | [bar] |

| | | |
|------------|-----------------------------|---------------------|
| p_{LP} | Suction port pressure | [bar] |
| Q_{HP} | pump discharge flow rate | [m ³ /s] |
| Q_{LK} | pump case flow rate | [m ³ /s] |
| Q_{LP} | pump suction flow rate | [m ³ /s] |
| Q_{rHPi} | piston discharge flow rate | [m ³ /s] |
| Q_{rLPi} | piston suction flow rate | [m ³ /s] |
| R | piston pitch radius | [m] |
| V_0 | piston volume at ODC | [m ³ /s] |
| V_D | piston dead volume | [m ³ /s] |
| x_i^h | upper limit for parameter i | - |
| x_i^l | lower limit for parameter i | - |
| z | number of pistons | - |

Acronym

| | |
|------|------------------------------|
| DCFV | Decompression filter volume |
| FBNS | Fluid borne noise source |
| IDC | Inner dead center |
| ODC | Outer dead center |
| PCFV | Precompression filter volume |
| SBNS | Structure borne noise source |

References

Ericson, L. 2008. *Flow Pulsations in Fluid Power Machines – a Measurement and Simulation Study*. PhD thesis. Linköping University, Linköping, Sweden.

Ivantysyn J. and Ivantysynova M. 2001. *Hydrostatic Pumps and Motors*. Academic Books International, New Delhi.

Ivantysynova, M., Seeniraj, G. K. and Huang, C. 2005. Comparison of different valve plate designs focusing on oscillating forces and flow pulsation. *The Ninth Scandinavian International Conference on Fluid Power, SICFP '05*, Linköping, Sweden.

Johansson, A. and Palmberg, J. O. 2005. The importance of suction timing in axial piston pumps. *The ninth Scandinavian International Conference on Fluid Power, SCIFP '05*, Linköping, Sweden.

Johansson, A. 2005. *Design Principles for Noise Reduction in Hydraulic Piston Pumps - Simulation, Optimisation and Experimental Verification*. PhD thesis, Linköping University, Linköping, Sweden.

Klop, R. and Ivantysynova, M. 2010. Sound Intensity Measurements to Investigate Noise Generation of Hydrostatic Transmissions. *Proceedings of the 7th International Fluid Power Conference Aachen 2010 (7th IFK)*, Vol. 2, pp. 229 - 242, Aachen, Germany.

Seeniraj, G. K. 2009. *Model Based Optimization of Axial Piston Machines Focusing on Noise and Efficiency*. PhD thesis. Purdue University, Indiana, USA.

Seeniraj, G. K. and Ivantysynova, M. 2011. A Multi-parameter Multi-objective Approach to Reduce Pump Noise Generation. *International Journal of Fluid Power*, March 2011, 12 (1), pp. 7 - 17.



Ganesh Kumar Seeniraj

Born on May 10, 1980 in Sivakasi, Tamil Nadu, India. He received his Bachelor of Engineering in Mechanical Engineering from College of Engineering, Guindy, Anna University, India in 2001. He received his MS in Mechanical Engineering from Kettering University, USA in 2003 and PhD from Purdue University, USA in 2009. Improving the efficiency of Fluid Power Systems at both component and system level has been his main research area. His research focus also includes reduction of fluid borne and structure borne noise source in hydraulic pumps/motors and transmissions.



Minming Zhao

Born on August 21st 1987 in Zhoushan, China. He received his BS degree in Mechanical Engineering in 2010 from Shanghai Jiao Tong University (SJTU), China. He is currently a master student at Purdue University. His main research focuses on configuration and control strategy for hydraulic hybrid transmission and reduction of fluid borne and structure borne noise sources in hydraulic pumps/motors and transmissions.



Monika Ivantysynova

Born on December 11th 1955 in Polenz (Germany). She received her MSc. Degree in Mechanical Engineering and her PhD. Degree in Fluid Power from the Slovak Technical University of Bratislava, Czechoslovakia. After 7 years in fluid power industry, she returned to university. In April 1996 she received a Professorship in fluid power & control at the University of Duisburg (Germany). From 1999 until August 2004 she was Professor of Mechatronic Systems at the Technical University of Hamburg-Harburg. Since August 2004 she is Professor in Mechanical Engineering and Agricultural and Biological Engineering at Purdue University, USA. She was approved as Maha named Professor in Fluid Power Systems and director of the Maha Fluid Power Research Center at Purdue University in November 2004. Her main research areas are energy saving actuator technology and model based optimization of displacement machines as well as modeling, simulation and testing of fluid power systems. Besides the book "Hydrostatic Pumps and Motors" published in German and English, she has published more than 90 papers in technical journals and at international conferences.